In Vivo Tracking of the Degradation of Mesoporous Silica through ^{89}Zr Radio Labelled Core-shell Nanoparticles

Elisa Bindini[§], Maria de los Angeles Ramirez[§], Xabier Rios, Unai Cossío, Cristina Simó, Vanessa Gomez-Vallejo, Galo Soler-Illia, Jordi Llop, Sergio Moya**

Dr. E.B. Author 1, M. A. R. Author 2, C.S. Author 5 and Dr. S.M Author 9
Soft Matter Nanotechnology Group, CIC biomaGUNE, Basque Research and Technology Alliance (BRTA), Paseo Miramón 182, 20014 San Sebastián, Guipúzcoa, Spain

M.A.R. Author 2 and Prof. G. S-I. Author 7
Instituto de Nanosistemas, UNSAM, CONICET, Avenida 25 de Mayo 1021, 1650 San Martín, Buenos Aires, Argentina

Dr. X.R. Author 3, Dr. U.C. Author 4, C.S. Author 5, Dr. V. G-V. Author 6 and Dr. J. L. Author 8
Radiochemistry and Nuclear Imaging Group, CIC biomaGUNE, Basque Research and Technology Alliance (BRTA), Paseo Miramón 182, 20014 San Sebastián, Guipúzcoa, Spain

Dr. J. L. Author 8
Centro de Investigación Biomédica en Red – Enfermedades Respiratorias (CIBERES), Av. Monforte de Lemos, 3-5, 28029 Madrid, Spain.

* Corresponding author E-mail: smoya@cicbiomagune.es
jllop@cicbiomagune.es

§ These authors contributed equally to this work.

Keywords: nanoparticles, in vivo imaging, nuclear chemistry, mesoporous materials, silica, degradation, biodistribution

ABSTRACT: While Mesoporous silica nanoparticles (MSNs) have been extensively studied as high-potential drug delivery platforms, the successful clinical translation of these nanocarriers strongly depends on their biodistribution, biodegradation and elimination patterns *in vivo*. In this work, we report a novel method to follow the *in vivo* degradation of MSNs by tracking a radioactive label embedded in the silica structure. Core-shell silica nanoparticles (NPs) with a dense core and a mesoporous shell are labelled with low quantities of the positron emitter ^{89}Zr, either in the dense core or in the mesoporous shell. In vivo Positron Emission Tomography (PET) imaging and ex vivo organ measurements reveal a remarkable difference in the ^{89}Zr biodistribution between the shell-labelled and the core-labelled NPs. Release of the radio-tracer from shell-labelled NPs is used as a probe of the extent of silica dissolution, and a prompt release of the radioisotope is observed, with partially excretion already in the first two hours post injection, and a slower accumulation in bones over time. On the other hand, when ^{89}Zr is embedded in the nanoparticle core, the biodistribution remains largely unchanged during the first 6 h. These findings indicate that MSNs have fast, hour-scale, degradation kinetics in vivo.

1. Introduction

Over the past few decades, nanomaterials have pushed forward the frontiers of diagnostics and therapy [1–9]. Many nanoparticle platforms have been exploited as drug delivery vehicles, such as inorganic nanoparticles[10], liposomes[11,12] and polymer NPs.[13,14] However, a major drawback for the biomedical application of nanoparticles is that often they are not biodegradable and have limited body clearance, accumulating in the body with undesired consequences. [15]

Amongst inorganic nanoparticles, mesoporous silica nanoparticles (MSNs) deserve special attention thanks to their uniform and tuneable pore size, large surface area, and easy functionalization of pores and surface.[16–20] The porous structure of MSNs can be chemically engineered by relatively simple methods and pores can be filled with several types of drugs[21–25] or therapeutics such as RNA[26], DNA[27], or proteins[28] for delivery. Silica is generally recognized as being safe by the U.S. Food and Drug Administration (FDA) [29] with silica-based nanocarriers undergoing clinical trials. [30,31] Several reports investigate the effect of size, shape and surface chemistry on MSNs biocompatibility and biodistribution.[32–39] MSNs have an advantage over other porous materials, as they can degrade under physiological conditions. Moreover, degradation plays a fundamental role in the delivery of encapsulated drugs[40]. Nevertheless, the mechanism and kinetics of degradation of MSNs in biologically relevant conditions are still controversial, as they largely depend on particle concentration, MSN size, morphology, porosity, degradation medium, and condensation degree. [41] Amorphous silica is unstable in aqueous environments and it hydrolyses forming soluble silicic acid and silicate oligomers. The kinetics of this reaction is limited by saturation as silica can nucleate and re-precipitate from saturated media, ceasing dissolution. [42,43] Moreover, this dynamic equilibrium may lead to pore obstruction in the case of mesoporous silica, further impacting on its degradation behaviour as the surface area will decrease. [43,45] In fact, one of the main parameters controlling the degradation kinetics of mesoporous silica is its surface area.[32,45,46] In addition, pH and temperature also greatly affect silica dissolution. [47,48] The different parameters involved in silica dissolution lead to a huge variety of possible scenarios and to inconsistent results for the kinetics of silica degradation in physiological buffers or biological media. Silica dissolution has been indeed reported to last between a few hours and several days depending on the experimental conditions and MSN properties.

In several studies MSN degradation was observed over 7-15 days, reaching a maximum rate in the first 2 days. [33,37,49–51] In other cases, MSNs were claimed to be stable over 20 days in simulated body fluid (SBF). [52] However, studies made on mesoporous thin films indicate degradation kinetics on the time scale of 2-6 hours.[42,46,53] These huge discrepancies are due to large extent to the large variability of particle concentration and medium composition in the different studies. In fact, as investigated by He *et al*. [45], MSNs display a rapid degradation phase in physiologic buffers that lasts approximately 2 h, dissolving from 35% to 85% of the starting material, depending on concentration. If the concentration of MSN is above the solubility limit of silica, 145 µg/mL in water at 37°C for silicic acid, [47] free silicon species saturation is quickly reached and the silica begins to re-precipitate, apparently halting the dissolution process. If the MSN concentration is far below the solubility limit for silica, re-precipitation is avoided, and MSNs degrade in a few hours. Working at 0.1 mg/mL, 85% of the starting MSN material is dissolved in 2 hours in SBF before re-precipitation occurs. However,

only 35% of the material is dissolved when working at 0.5 mg/mL.[45] In many MSN studies related to stability, the working concentration is generally above 0.1 mg/mL, often approaching 1 mg/mL, which may explain the reported stability of several days.

A fundamental issue when studying the degradation of drug delivery vehicles, is to consider final conditions in a biological environment. If MSNs are injected to animals, the concentrations employed are always very far from saturation conditions, typically 0.02-0.08 mg/mL. Moreover, *in vivo,* nanoparticles are exposed to a flowing media, which removes products of dissolution and should reduce re-precipitation and aggregation. Therefore, we might expect *in vivo* degradation behaviour on an hour-scale, probably impeded with respect to SBF by the presence of proteins and other biomolecules that adsorb onto the particle surface (see Table 1). [46,49]

Table 1: Estimated degradation kinetics of mesoporous silica in vivo compared to the degradation kinetics of mesoporous silica in vitro, according to the main studies reported in literature. Some works, important to understand the degradation mechanism, aren't included in this table because they didn't provide easy quantification of the amount of degraded silica.

Material	Concentration (mg/mL)	Degradation (%)	Time (hours)	Media	Ref.
NPs (MCM-41)	0.48-10[a]	4	1-10	SBF[b]	43
NPs	0.2[a]	90	48	SBF	33
NPs	2[a]		24	SBF	37
NPs	1[a]	55	10 days	PBS	38
NPs	0.35[a]	20	20 days	SBF[c]	52
NPs (MCM-41)	< 0.1[d] 0.1 0.5[a]	100 85 35	2 2 2	SBF	45
Thin films	0.015[d]	85 35	1-2 3	PBS PBS+BSA	46
Thin films	0.04[d]	70 80	2 2	PBS DMEM+10%FBS	53
Estimated degradation					
NPs	0.07[d,e]	-[f]	2-24h	In vivo	

a) Above saturation (0.15 mg/mL)
b) In SBF, silicates of Ca and Mg precipitate onto the NPs surface in the first hours, passivating it and obstructing the pores, delaying the degradation process.
c) Experiments were performed at pH 5.5 where silica degradation is slower than at neutral pH.
d) Below saturation (0.15 mg/mL)
e) Concentration employed in the present work.

f) We could expect a degradation process taking place in the first hours post-injection but estimating the % of degradation of NPs In vivo isn't easy, because NPs uptake in organs greatly complicate the degradation patterns.

All studies carried out on MSN degradation up to now have been performed *in vitro*, trying to simulate *in vivo* conditions. Despite almost 20 years of MSN related studies, investigations focused on *in vivo* degradation of MSNs for drug delivery can be hardly found in the literature. The uncertainty surrounding their degradation behaviour is greatly restricting MSN translation from laboratories to clinical use. There are several *in vivo* studies on biodistribution and clearance of MSNs[18,20,39,54–56,59-60], but to the best of our knowledge, no dedicated work addressing MSN degradability *in vivo* has been reported until now. Monitoring MSN degradation *in vivo* following systemic delivery poses several technical difficulties. The *in vivo* visualization and quantification of nanomaterials is highly non-trivial. Techniques like Inducted Coupled Mass Spectroscopy (ICP-MS), which is frequently used for the quantification of element content in organs, require animal sacrifice and are not capable of distinguishing particulate silica from ions, providing information only on the total silica content. Fluorescence imaging can be used for tracing fluorescently labelled NPs *in vivo*; however, it is not quantitative and is difficult to translate to large animal species or humans.
For a quantitative evaluation of the distribution of NPs in bodily organs *in vivo*, nuclear imaging techniques such as Positron Emission Tomography (PET) or Single Photon Emission Computerized Tomography (SPECT), which detect activity from radionuclides incorporated in the NPs or linked to their surface, are ideally suited. Relative activity per organ can be related to the amount of nanomaterials in the organ from an initial dose/activity supplied. However, nanomaterial imaging/quantification in PET/SPECT relies on the fact that the tracer is always associated with the NPs. *A priori*, PET/SPECT techniques cannot distinguish between free radionuclide and the radionuclide associated with the NPs. However, one can expect that the biodistribution of detached radionuclides in the form of ions or organic molecules may significantly differ from that of the labelled NPs. Hence, a means to distinguish between free radionuclide coming from dissolution of the mesoporous NPs and radionuclide bound to the mesoporous nanoparticles (not dissolved MSNs) would be to ensure that in one case the nanoparticle does not dissolve, thereby providing information on nanoparticle biodistribution, while in the other it does dissolve. As the silica dissolution rate depends on surface area, mesoporous silica degrades much faster than dense silica. A core shell nanoparticle with a core of dense silica and a shell of mesoporous silica, which could be either labelled in the core or in the shell, could provide a means to distinguish between free and nanoparticle bound radionuclide. Radiolabelling at the core would provide information about the biodistribution of the nanoparticles, and if the radionuclide is located in the mesoporous shell, a different pattern of biodistribution from the core would mean that the mesoporous structure has

degraded. Based on this idea, we prepared core-shell nanoparticles with a dense silica core and a mesoporous shell, and we labelled either the core or the shell with Zirconium-89 (^{89}Zr) as sketched in **Figure 1a**. This positron emitter ($t_{1/2}$ = 78.4 h, positron energy β^+_{avg} = 396 keV) is particularly suitable for chelator-free labelling of silica. This is because Zr can integrate with the network of silica[57,58] and it bonds easily to the surface silanols following chelator-free labelling procedures.[59–61] Core shell MSNs with ^{89}Zr on the core, and core shell MSNs with the label in the shell are identical, differing only in the location of the label and can be expected to have the same fate. By designing this core shell labelling strategy, we show that we are able to discriminate the fate of the nanoparticle from that of the degradation products. Our results provide a first *in vivo* evaluation of the degradation of mesoporous silica and introduce fundamental knowledge for the design and evaluation of the drug delivery potential of mesoporous materials.

2. Results and Discussion

2.1 Morphology and Mesostructure of Core and Core-Shell silica particles

Transmission electron microscopy (TEM) images of dense core silica nanoparticles clearly indicate that they have uniform nanoparticle sizes with a diameter of about 40 nm and a regular spherical morphology (**Figure 1b**, left and **Figure S1**). Following the synthesis of the dense core, a mesoporous shell was fabricated via a standard templated sol-gel approach, resulting in a clear core-shell structure (**Figure 1b**, middle and right and **Figure S2**), where the 40 nm silica core is coated with a 20 nm shell of mesoporous silica. The size of core-shell nanoparticles is 80 nm in diameter, with a small percentage of the multi-core nanoparticles approaching 120 nm. Still, these nanoparticles remain in the size-range in which rapid lung and spleen accumulation *in vivo* is limited.[62] The mesoporous structure, visible by TEM, was confirmed by nitrogen adsorption-desorption isotherms, which showed an average pore diameter of 2.5 nm (**Figure S4**), typical of CTAB-templated materials. The calculated Brunauer-Emmett-Teller (BET) surface area was 188 m^2/g.

The synthesized core-shell NPs were coated with a PEG layer, using (3-aminopropyl)triethoxysilane (APTES) as the silane coupling agent to incorporate active amine groups on the silica surface. These

APTES-coated nanoparticles were then reacted with *N*-succinimidyl ester of hydroxyl poly(ethylene glycol) (HO-PEG5K-NHS) .

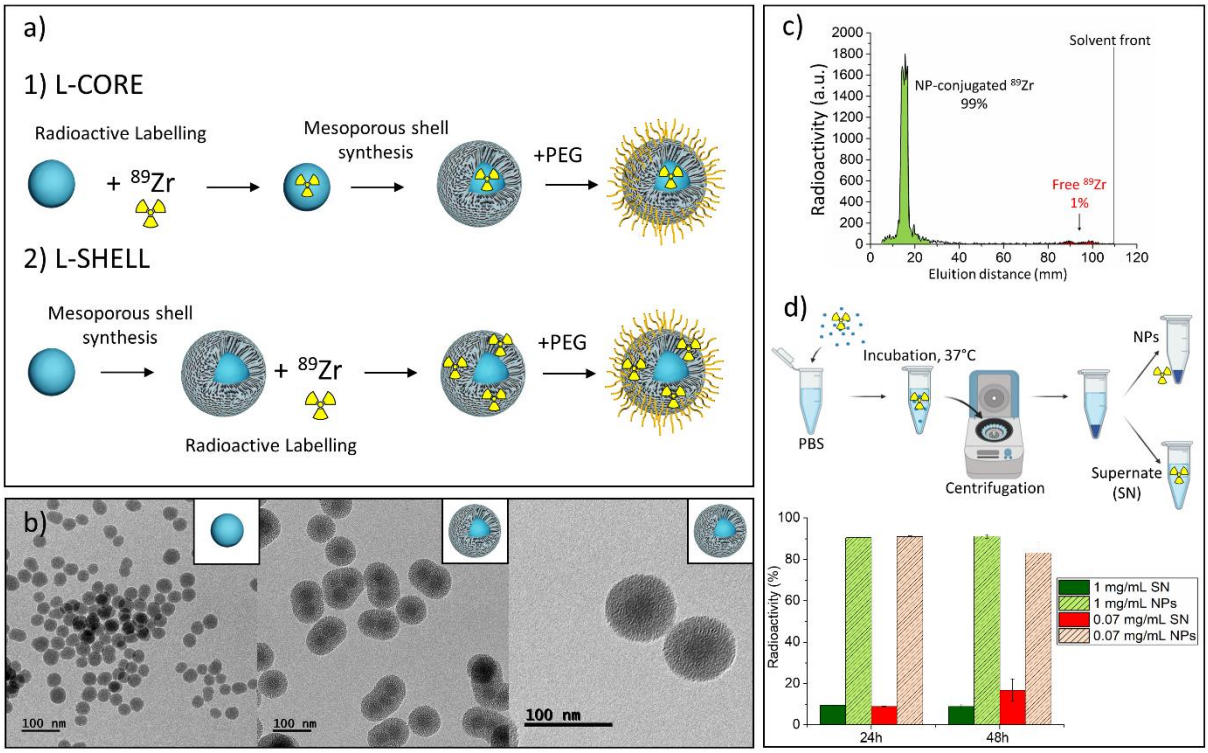

Figure 1: : Synthesis and characterization of ^{89}Zr labelled core-shell SiO_2 nanoparticles: ***a)*** *Scheme of the multi-step synthesis of L-CORE and L-SHELL NPs;* ***b)*** *TEM images of the dense silica core and the core-shell NPs;* ***c)*** *iTLC chromatogram of ^{89}Zr labelling reaction, using EDTA 50mM (pH=5) as eluent. Non-bound ^{89}Zr is eluted with the solvent while ^{89}Zr bound to nanoparticles is retained with NPs on the silica thin layer;* ***d)*** *Radiochemical stability test in PBS, 37°C. Green colours represent 1 mg/mL concentration of NPs, red colours represent 0.07 mg/mL. Patterned bars represent radioactivity values of nanoparticles, while non-patterned bars are chosen for supernatant.*

2.2 Chelator-Free ^{89}Zr Labelling and *In vitro* stability tests

The chelator-free labelling procedure relies on the strong interaction between deprotonated silanol groups present on the silica surface (hard Lewis base) and the Zr^{4+} ions (hard Lewis acid) to ensure stable labelling of silica without the use of organic linkers, which may be cleaved *in vivo*. Labelling conditions were chosen according to reported studies of ^{89}Zr labelling on silica MSNs, which evidenced a dependence on time and temperature of the labelling yield[59].Our results show that about 99% ^{89}Zr labelling yield was achieved after 1h of incubation in HEPES at 70° C (**Figure 1c**).
In order to perform the *in vivo* investigation of the degradation process, we prepared two different batches of nanoparticles. The first batch (core-labelled; from now on, L-CORE) incorporated the radionuclide ^{89}Zr on the dense core, i.e. dense silica NPs were exposed to ^{89}Zr before the shell synthesis; while the second batch of particles (shell-labelled; from now on, L-SHELL) was labelled via incorporation of the radionuclide in the mesoporous shell i.e. after the synthesis of core shell NPs. To

verify the radiochemical stability of the radiolabelled nanoparticles, L-SHELL NPs were suspended in PBS at 37 °C for 24 h and 48 h, under shaking. After this treatment, > 90% of the starting radioactivity (decay-corrected) was found on the nanoparticles and only 10% was found in the supernatant after 24 h, even at a NP concentration of 0.07 mg/mL (i.e., slightly below saturation), as shown in **Figure 1d**. After 48 h, the percentage of radionuclide attached to the NPs remains unaltered at 1 mg/mL (above saturation limit), while a slight release is observed at 0.07 mg/mL (below saturation limit), probably due to partial silica dissolution. These results suggest that the radiolabelling strategy is robust and the radionuclide does not easily leach away unless the nanoparticle degrades. Following these results, the presence of free Zr *in vivo* can be directly correlated with silica dissolution, as the radionuclide is not released from intact nanoparticles but can be detected in the supernatant when degradation of mesoporous silica occurs.

2.3 *In vivo* degradation and biodistribution study

Next, we tackled the investigation of the degradation of the NPs *in vivo*, using L-SHELL and L-CORE NPs. Based on the extensive literature on mesoporous silica degradation, a fast silica hydrolysis *in vivo* during the first 24 hours post-injection could be expected.

The labelled NPs were injected intravenously and PET imaging sessions were carried out at different times after administration. Visual inspection of PET images showed a different distribution profile for L-CORE and L-SHELL nanoparticles (**Figure 2**). Coronal maximum intensity projections (MIP) PET images obtained at t=10 min and 2 h periods clearly show that irrespectively of the position of the radiolabel and the time point, major uptake occurs in the liver and the spleen, as expected for NPs in this size range, due to sequestration and retention by the Mononuclear Phagocytic System. However, at longer times (24 hrs and 48 hrs after administration) mice injected with L-SHELL particles clearly show accumulation of radioactivity in the bones, as observed in axial slices. Additionally, accumulation of radioactivity in the lungs was also observed at t=10 min and 2 h. Instead, mice injected with L-CORE nanoparticles do not show any visible accumulation of radioactivity in the bones or any organs other than the spleen and liver over the whole duration of the study. The presence of ^{89}Zr in bones after administration of L-SHELL nanoparticles is indicative of the shell degradation and consequent release of the radionuclide, as: (i) Previous works have demonstrated that the free ^{89}Zr is preferentially uptaken in bones, where it binds to phosphates[63], while NPs do not accumulate in bones[56]; and (ii) ^{89}Zr-labelled nanoparticles showed excellent stability *in vitro* (see above), thus confirming that the release of ^{89}Zr without degradation of the shell, by diffusion, is minimal. Our results clearly point out that ^{89}Zr release and accumulation in bones can be employed as an indicator of silica dissolution kinetics.

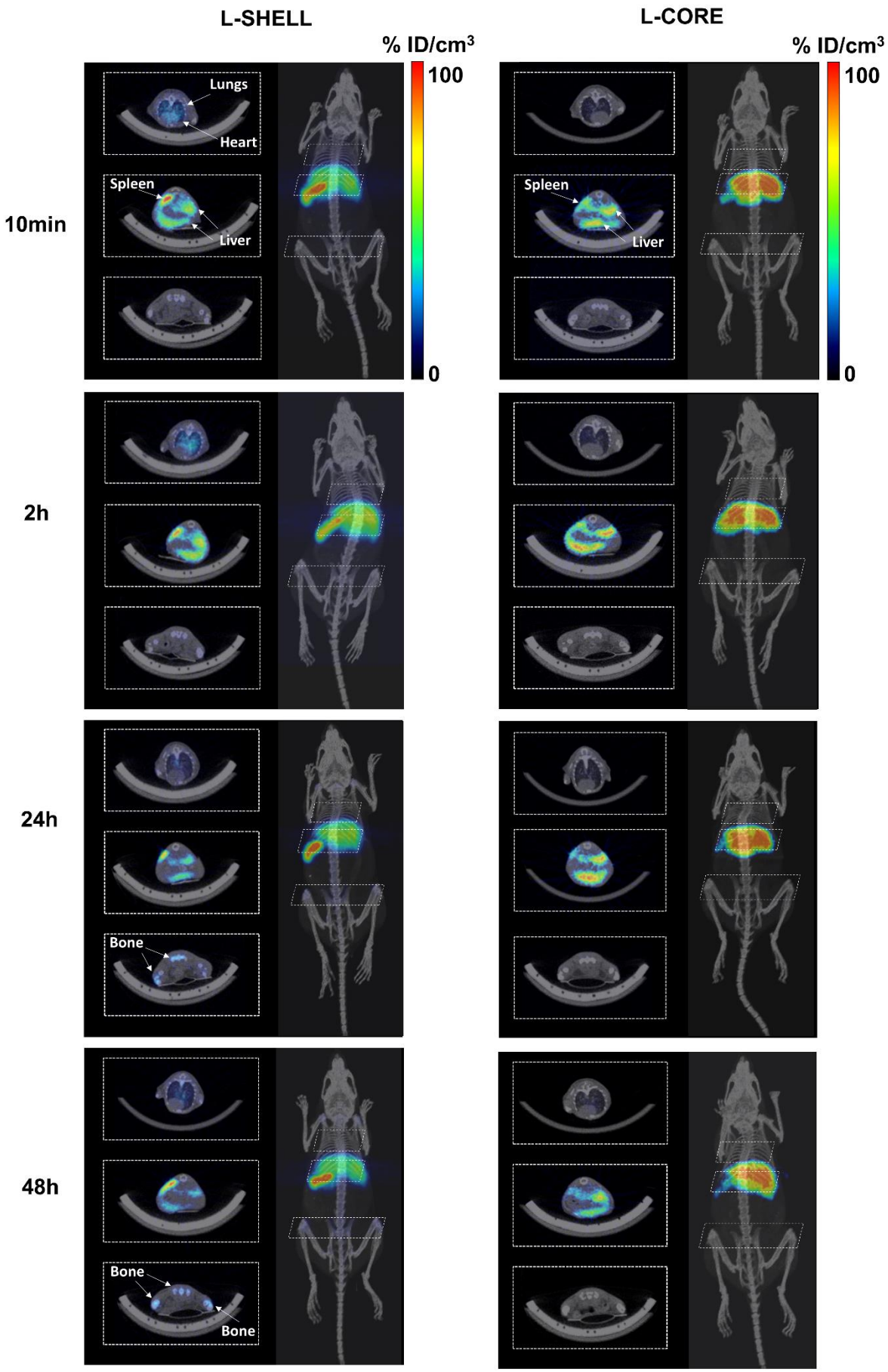
L-SHELL
L-CORE
% ID/cm3
100
0
10min
2h
24h
48h
Lungs
Heart
Spleen
Liver
Bone

Figure 2: PET/CT images of mice injected with L-SHELL particles (left) and L-CORE particles (right) after 10 min, 2h, 24h and 48 h from injection. For each time point and type of NP, whole body coronal PET maximum intensity projections have been co-registered with 3D rendered CT images. Representative axial slices, co-registered with the corresponding CT slices, are also shown. Color scale bars refer to coronal images.

In order to acquire accurate quantitative data on MSN degradation, we combined *in vivo* imaging with *ex vivo* studies. With that aim, animals were injected intravenously with either L-CORE or L-SHELL NPs and sacrificed at different time points:10 min, 2h, 6h, 24h and 48h, post injection. Organs were harvested and the concentration of radioactivity in each organ was determined by gamma counting (**Figure 3**). As expected, and correlating with PET results, the highest amount of radioactivity was found in the liver and the spleen, irrespectively of the position of the label, due to sequestration by the Mononuclear Phagocytic System; minor accumulation was observed in the heart and kidneys[62,64–67]. Significant differences between L-CORE and L-SHELL nanoparticles were observed for the heart, the intestine, the kidneys and the lungs. While low uptake values in these organs are observed for L-CORE NPs, significantly higher values were observed for L-SHELL, peaking at 10 min (heart, intestine and kidneys) and 2h (lungs) after administration and progressively decreasing afterwards. These results suggest that, in the case of L-SHELL nanoparticles, ^{89}Zr is rapidly distributed in the blood and accumulated at short times mainly in the intestine and kidneys, and to lesser extend in the lungs. After two hours, activity decreases in the intestine and kidneys while it increases in the lungs. At longer times activity significantly decreases, remaining practically constant for L-SHELL NPs, prior to elimination and/or ^{89}Zr activity accumulation in the bones. As the degradation of the mesoporous silica shell does not affect ^{89}Zr stability for L-CORE nanoparticles, we observe very stable values in all organs in the case of core-labelled nanoparticles.

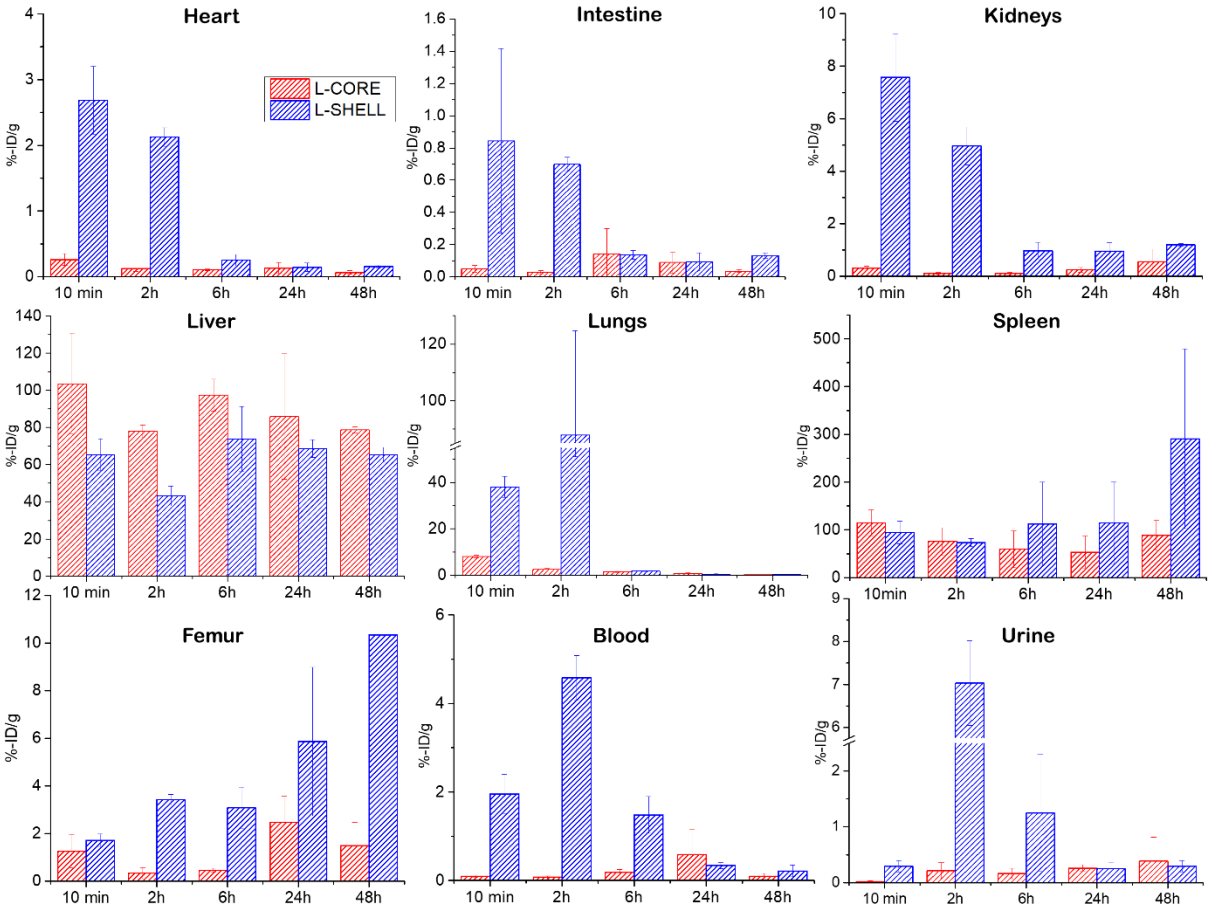

Figure 3: Percentage of injected dose per gram of organ. Results from ex-vivo measurements by γ-counter. Values are represented in red for L-CORE nanoparticles and in blue for L-SHELL nanoparticles.

A closer look at the values found in urine and bones (**Figure 3**) reveal some interesting trends. The presence of radioactivity in both urine and bones is a consequence of nanoparticle degradation, as intact nanoparticles do not accumulate in the bones and they are above the glomerular filtration limit of the kidneys. In urine, the concentration of radioactivity is very low over 48 hours when L-CORE nanoparticles are administered, due to the slow degradation and release kinetics of the core to which ^{89}Zr is anchored. On the contrary, after intravenous injection of L-SHELL nanoparticles, a peak of radioactivity in urine is observed at 2h after administration, confirming that a large amount of ^{89}Zr is released and excreted by the urinary system. A similar trend is observed in blood. Nanoparticle circulation in the blood stream is equivalent for both L-CORE and L-SHELL nanoparticles, since both L-CORE and L-SHELL are identical apart from the position of the label and both were administrated in equal activity doses and by the same administration route. Therefore, the higher presence of radioactivity in the blood for L-SHELL nanoparticles can only be explained as a consequence of the release of ^{89}Zr associated to mesoporous silica degradation from nanoparticles accumulated in other organs.

It is interesting to note that radioactivity in the femur follows an inverse trend when compared to urine and blood. While radioactivity in blood peaks at t=2h after administration, activity in bones progressively increases over time. Our results support that *in vivo*, mesoporous silica degradation is fast. During the first two hours post-injection, a consistent amount of ^{89}Zr is released and enters the blood stream. The radionuclide translocates to different organs such as the heart, lungs and kidneys at short times after administration, and progressively accumulates in the bones over time, as previously reported.[63] A large amount of the radionuclide is also quickly excreted through the urinary system. Our data are consistent with literature reports on MSNs excretion by renal clearance. This clearance pathway is rapid with high percentages of silica degradation products found in the urine of injected mice after 30 minutes,[62] demonstrating that MSNs are indeed biodegradable *in vivo* with a fast hour-scale kinetics, as expected from *in vitro* data for low concentrations. Lu and co-workers found that Si content in urine decreases with time, confirming fast renal clearance in the first 24 hours. They also found that 94.4% of injected Si was excreted within 4 days through urine and feces.[64] Moghaddan and co-workers found that around 20% of injected MSNs were excreted by urine in the first 24 hours.[39]

Analysing the percentage of injected dose (ID) for every organ (without normalising for the organ weight) global trends of biodistribution became evident (**Figure 4**). When ^{89}Zr is embedded in the mesoporous shell, after 10 minutes we observe 23 % of the ID in the liver, 9 % in the spleen and 4 % in the lungs. After two hours, the radioactivity decreases to 17.5 % of the ID and to 7 % of the ID, respectively, in the liver and spleen, and increases to 8.5 % of the ID in the lungs. An increase is also seen in the blood and in the femur. From these data we can infer that MSNs become trapped in the liver and spleen in the very first minutes and start to degrade there. The degradation products are then released and transferred to the blood, to be subsequently excreted by urine. The radionuclide ^{89}Zr is released along with silicate species and we can follow its increase in the blood after two hours and its diminished presence in the liver and spleen. Well-perfused blood-filled organs, such as the lungs, show enhanced accumulation of the radionuclide, which likely remains anchored to nanoparticle fragments or silicate oligomers derived from NP degradation. As already observed by He *et al*.,[62] silica has a remarkable uptake in lung tissue at short times. When MSN fragments circulate for some hours they are sent back to the liver and spleen to be excreted and we can observe an increase to 26.5 % of the ID in the liver and to 9 % in the spleen 6 hours post injection. After this long circulation time the lungs are found to be almost completely clear of ^{89}Zr, which begins to accumulate in the bones. This behaviour may be attributed to the fast transfer of nanoparticle fragments from the lungs to other tissues under the high local hemoperfusion rate. After 24h and

48h we observe a progressive decrease in activity in the liver due to MSN degradation and clearance, along with progressive accumulation of free ^{89}Zr in bones.

On the other hand, when ^{89}Zr is embedded in the core of the nanoparticles, the biodistribution remains largely unchanged in the first 6 h. Following an initially rapid uptake in the liver and spleen, mesoporous silica must degrade, and follow the excretion path from the liver to blood and urine and from circulating blood back to the liver. However, as ^{89}Zr is unaffected by mesoporous silica degradation we do not observe any change in the radioactivity biodistribution. After 24h and 48h a global decrease in % ID indicates that the core begins to degrade and the majority of ^{89}Zr is likely excreted through urine and recirculates from the blood to the spleen and liver. This can be seen as only a slight increase is found in the bones, while the % ID rises in the liver and spleen. In fact, the accumulation of the radionuclide in the bones seems to take more time, as evidenced by the L-SHELL data. Nevertheless, Chen et al. [59] found that the localization of ^{89}Zr on the surface of dense particles results in a faster release of the ^{89}Zr in vivo than for the mesoporous particles labelled with the same radioisotope. In our case, after labelling the dense silica we assemble a mesoporous shell on top, which gives additional stability to ^{89}Zr, which is trapped between the shell and the core. We expect that the release of ^{89}Zr will only take place when the mesoporous shell is degraded and that the slow release observed for L-CORE is due mainly to the ^{89}Zr position trapped between core and shell. In the study cited in ref. 59 the mesoporous nanoparticles show a very stable radiolabelling, retaining the activity in the liver for several days. Authors used MSNs of 150 nm, with long radial pores, in which ^{89}Zr can penetrate in depth during the labelling procedure. In these conditions ^{89}Zr is confined in the mesopores, resulting in a more stable labelling. We also observe a high stability for the ^{89}Zr labelling *in vitro*, with the isotope being released only in conditions allowing the degradation of the mesoporous shell. The differences in the ^{89}Zr release kinetics in vivo between our NPs and the ones employed in ref. 59 can be ascribed to the different size of the NPs (larger NPs are more easily retained in the liver) and also to the depth of the mesopore structure. In fact, the mesoporous layer thickness is important because during the labelling procedure ^{89}Zr diffuses and binds to the surface inside the mesopores. Our nanoparticles present a very thin mesoporous shell of 20 nm that degrades much faster than a 150 nm particle, releasing ^{89}Zr in shorter times. Moreover, differently from our nanoparticles, mesoporous NPs were not PEGylated in Chen's work. The absence of PEG on the NPs probably results in the accumulation of proteins around the NPs, with consequent capping of the pores, both in vitro, in plasma, and the in vivo experiments. This phenomenon could greatly affect the silica degradation kinetics[45,48] and the consequent ^{89}Zr release, hindering both processes. We assume that this is the main reason for the high stability and apparent absence of degradation of the mesoporous NPs reported in ref. 59. In our work, PEGylation prevents the uptake of proteins but

clearly allows for the diffusion of smaller molecules from the culture medium and degradation products.

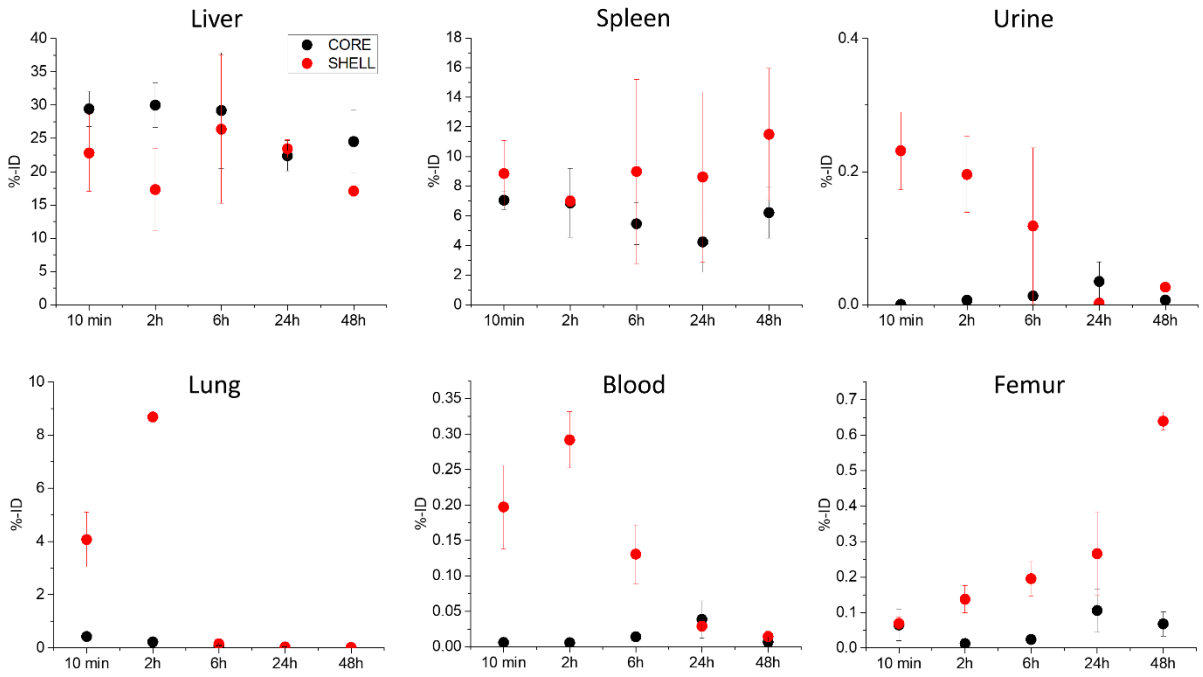

Figure 4: Percentage of injected dose (ID) for different organs: for L-SHELL nanoparticles (red dots) and for L-CORE nanoparticles (black dots). The values for blood have been calculated from the measured %ID/g, considering an average blood volume of 70 mL/kg and a blood density of 1.057 g/mL. The values measured in urine have to be considered qualitatively, as they can greatly vary depending from the sampling (before or after mouse urination).

3. Conclusion

The *in vivo* degradation of MSNs has been investigated through radioactive labelling with ^{89}Zr in two groups of identical core-shell nanoparticles, composed of a dense silica core and a mesoporous silica shell, with the radiolabel localised either in the core or in the shell. When the label is located in the mesoporous shell, the radioisotope is released promptly, following the silica degradation kinetics. When the core is labelled, the location of the radionuclide is unaffected by shell degradation and it co-localises with the nanoparticle core. Nanoparticles are rapidly uptaken in the liver and spleen, and readily begin to degrade into silica fragments and silicate oligomers. These degradation products are transferred to the blood and are partially excreted through urine and partially re-circulated in the blood stream to the lungs before finally translocating back to the spleen and liver. This behaviour is evidenced in the first 6 hours after the injection of L-SHELL nanoparticles, following the pathway of ^{89}Zr that is released along with the nanoparticle fragments. We can state that the radioactive label is signalling the position of the degradation products and not the nanoparticles because L-CORE

nanoparticles follow a different clearance pathway, as evidenced by the stable % ID in the liver and spleen over 6 hours. After 24 hours from the administration of L-SHELL NPs we could detect radioactivity in the bones, which further increased at 48h post injection, resulting from ^{89}Zr accumulation. Following administration of L-CORE, only a slight increase in radioactivity is observed in the femur after 24h and 48h by *ex-vivo* measurements. These results point to a rapid *in vivo* MSN degradation that can already be seen at 2h post-injection. We tackle here a fundamental aspect for the use of mesoporous silica NPs for biomedical application, such as their *in vivo* degradation kinetics; these results are of paramount importance to design efficient MSNs platforms for drug delivering and for targeting specific tissues, allowing to better control the drug release kinetics.

4. Experimental Section

Synthesis of dense SiO_2 cores ($dSiO_2$): Uniform ~40 nm sized dense silica NPs were prepared using a Stöber method. Briefly, water (5 mL) was mixed with absolute ethanol (35 mL) and NH_3 solution (25%) (0.8 mL) and the mixture was stirred 20 minutes at 50 °C. Then, TEOS (1 mL) was added dropwise during one minute and the reaction was kept under stirring at 50°C for 1h. Nanoparticles were collected by centrifugation (13400 rpm, 15min), washed with ethanol (x3) and dried 72 h at 60°C.

Synthesis of mesoporous silica shell $dSiO_2$@$mSiO_2$: 2 mg of $dSiO_2$ were suspended in a solution of ethanol (300 µL) and water (600 µL). CTAB was added (4.5 mg) and the mixture was left under stirring at r.t. for 20 minutes. Afterwards, ammonia (10 µL) and TEOS (8 µL) were added sequentially, under stirring. After 45 minutes, nanoparticles were collected by centrifugation (10000 rpm, 10 min.) and washed with ethanol (x2). To remove CTAB, nanoparticles were sonicated in a NH_4NO_3 solution in ethanol (6g/L) for 5 minutes (x3) and washed with ethanol (x2). To remove aggregates that may form during the reaction a fast spin (3000 rpm, 2 min) was performed, collecting the supernatant only. An aliquot of the colloid was dried (overnight at 60 °C) and weight to calculate the concentration and nanoparticles were kept in absolute ethanol until use.

Synthesis of $dSiO_2$@$mSiO_2$-APTES: A solution of APTES in dry ethanol 0.1% v/v was prepared and kept under inert atmosphere. The $dSiO_2$@$mSiO_2$ were suspended in dry ethanol at a concentration of 1 mg/mL and 10 µL of APTES solution 0.1% were added for each mg of NPs. Reaction was left stirring 4h at r.t. under inert atmosphere. Nanoparticles were collected by centrifugation and washed with ethanol (x3). Successful grafting of APTES was checked by Z-potential measurements (SI).

^{89}Zr labelling: [^{89}Zr]ZrC_2O_4 was produced in house following a standard protocol. The as-obtained 500 µL of 1 M oxalic acid containing ^{89}Zr (10.85 mCi, 401.5 MBq) were neutralized with 2 M sodium carbonate until pH 7-8 and the volume was adjusted to 1 mL with 0.5 M HEPES buffer (pH 7.4). 2 mg of the silica NPs (dSiO2 or $dSiO_2$@$mSiO_2$-APTES) were dispersed in 700 µL of 0.5 M HEPES buffer and 500 µL of the freshly prepared ^{89}Zr solution were added and well mixed. The mixture was left to react 1h at 70°C. A drop of the reaction mixture was used to perform instant thin layer chromatography (iTLC), to verify the labelling yield. Stripes from commercially available instant thin layer chromatography paper impregnated with silica gel (ITLC-SG: Agilent) were used as a stationary phase and EDTA 50 mM (pH=5) was used as mobile phase, measurements were made with a MiniGITA* TLC instrument. Afterwards, nanoparticles were collected by centrifugation (13400 rpm, 10 min) and washed with water (x3) to remove non-bound ^{89}Zr. **Shell-labelled (L-SHELL)** NPs were synthesized "in cold" conditions (without the addition of radionuclide) until the APTES grafting stage, then the label (^{89}Zr) was incorporated in the mesoporous shell, followed by PEG grafting. For **core-labelled (L-CORE)** NPs the dense silica core was labelled with ^{89}Zr before the mesoporous shell synthesis and subsequent APTES and PEG grafting.

Synthesis of $dSiO_2$@$mSiO_2$-PEG: 2 mg $dSiO_2$@$mSiO_2$-APTES were suspended in PBS 10 mM pH 7.4 (2mL). NHS-PEG5K-OH (500 µg) was added and the reaction was left shaking (600 rpm) at r.t. for 45-60 minutes. Nanoparticles were then collected by centrifugation and washed with PBS (x3).

Nanoparticles were kept in ethanol until use. They were centrifuged and re-dispersed in PBS before injection.

NPs were imaged by transmission electron microscopy (TEM) operated on a LaB6-TEM of type JEOL JEM-1400PLUS (40kV - 120kV, HC pole piece) equipped with a GATAN US1000 CCD camera (2k x 2k).

Radio-labelling stability test: dSiO2@mSiO2-PEG labelled with ^{89}Zr were suspended in 500 uL of PBS at 1 mg/mL and 0.07 mg/mL concentration. Samples triplicates were made and the radioactivity of each sample was measured. Nanoparticles were left shaking (630 rpm) at 37°C for 24h and 48h. Nanoparticles and supernatant were separated by centrifugation, collected and measured by an automatic γ-counter (2470 Wizard, Perkin Elmer) for radioactivity.

In vivo PET imaging of ^{89}Zr labelled dSiO$_2$@mSiO$_2$-PEG: Animals were maintained and handled in accordance with the Guidelines for Accommodation and Care of Animals (European Convention for the Protection of Vertebrate Animals Used for Experimental and Other Scientific Purposes). All animal procedures were performed in accordance with the Spanish policy for animal protection (RD53/2013), which meets the requirements of the European Union Animal Directive (2010/63/EU). Experimental procedures were approved by Ethical Committee of CIC biomaGUNE.

The final injections (100 µL, 1 mg/mL) were performed intravenously via the tail vein of healthy female mice (C57BL/6) which were anesthetized with 3-5% isoflurane (IsoFlo®, Abbot Laboratories, Lake Bluff, IL, USA) in pure O_2. The average injected activity was 120 µCi (4.4 MBq). After administration, mice were placed on the eXplore Vista-CT scanner (GE Healthcare, Chicago, IL, USA) and static PET images were acquired at t=10 min, 2h, 6h, 24h and 48h time points. Two bed positions were defined in all cases to acquire whole body images. After each PET acquisition, a CT scan (X-Ray energy: 40 kV, intensity: 140 µA) was performed for a later attenuation correction application in the image reconstruction, as well as for unambiguous localization of the radioactive signal. Random and

scatter corrections were also applied to the reconstructed image (filtered back projection reconstruction algorithm was used to reconstruct all datasets). After reconstruction, PET images were analyzed using PMOD image analysis software (PMOD Technologies Ltd, Zurich, Switzerland).

In vivo biodistribution study of ^{89}Zr labelled dSiO$_2$@mSiO$_2$-PEG: The average injected activity was 65 µCi (24.1 MBq) for shell-labelled NPs and 41 µCi (15.2 MBq) for core-labelled NPs. The average injected quantity was around 85 µg of NPs for each animal. Animals were anesthetized by isofluorane gas and sacrificed at 10', 2h, 6h, 24h and 48 h post injection and organs were removed, weighed and counted in a gamma counter for ^{89}Zr activity. The percent injected dose per gram (%ID/g) for each organ was computed by normalization to the total activity injected (decay-corrected).

Supporting Information

Supporting Information is available from the Wiley Online Library or from the author.

Acknowledgements

S.E. Moya and J. Llop thank the MAT2017-88752-R and CTQ2017-87637-R Retos projects, respectively, from the Ministerio de Economía, Industria y Competitividad, gobierno de España; G. J. A. A. Soler-. Illia acknowledges support from ANPCyT (PICT 2015-2526 and PICT 2018-4651). This work was performed under the Maria de Maeztu Units of Excellence Program from the Spanish State Research Agency – Grant No. MDM-2017-0720.

Author Information

These authors contributed equally: Elisa Bindini and Maria de los Angeles Ramirez.

Author Contributions

E.B., M.A.R., S.M., J.L. and G.S.-I. conceived and designed the study. E.B. and M.A.R. synthesized and characterized mesoporous nanoparticles, performed the radioactive labelling and the ex-vivo experiments. X.R. supervised the radio-labelling experiments and the ex-vivo experiments and performed the animal sacrifices. U.C. performed PET/CT scans. C.S. analyzed PET/CT data. V.G.-V.

organized and supervised animal experiments. E.B, M.A.R., S.M., and J.L. analyzed and discussed the data. E.B., S.M., and J.L. contributed to the writing of this paper. All authors have read and approved the final manuscript.

References

[1] H. Shao, T.-J. Yoon, M. Liong, R. Weissleder, H. Lee, *Beilstein J Nanotechnol* **2010**, *1*, 142.

[2] S. Prijic, G. Sersa, *Radiology and Oncology* **2011**, *45*, 1.

[3] L. Cong, M. Takeda, Y. Hamanaka, K. Gonda, M. Watanabe, M. Kumasaka, Y. Kobayashi, M. Kobayashi, N. Ohuchi, *PLOS ONE* **2010**, *5*, e13167.

[4] J. E. Fuller, G. T. Zugates, L. S. Ferreira, H. S. Ow, N. N. Nguyen, U. B. Wiesner, R. S. Langer, *Biomaterials* **2008**, *29*, 1526.

[5] M. N. Rhyner, A. M. Smith, X. Gao, H. Mao, L. Yang, S. Nie, *Nanomedicine* **2006**, *1*, 209.

[6] X. Gao, Y. Cui, R. M. Levenson, L. W. K. Chung, S. Nie, *Nat Biotechnol* **2004**, *22*, 969.

[7] E. Boisselier, D. Astruc, *Chem. Soc. Rev.* **2009**, *38*, 1759.

[8] L. R. Hirsch, R. J. Stafford, J. A. Bankson, S. R. Sershen, B. Rivera, R. E. Price, J. D. Hazle, N. J. Halas, J. L. West, *Proceedings of the National Academy of Sciences* **2003**, *100*, 13549.

[9] C. J. Gannon, C. Patra, R. Bhattacharya, P. Mukherjee, S. A. Curley, *Journal of Nanobiotechnology* **2008**, *6*, 2.

[10] R. Liang, M. Wei, D. G. Evans, X. Duan, *Chem. Commun.* **2014**, *50*, 14071.

[11] M. Alhariri, A. Azghani, A. Omri, *Expert Opinion on Drug Delivery* **2013**, *10*, 1515.

[12] P. P. Deshpande, S. Biswas, V. P. Torchilin, *Nanomedicine* **2013**, *8*, 1509.

[13] N. Doshi, S. Mitragotri, *Advanced Functional Materials* **2009**, *19*, 3843.

[14] W. B. Liechty, D. R. Kryscio, B. V. Slaughter, N. A. Peppas, *Annual Review of Chemical and Biomolecular Engineering* **2010**, *1*, 149.

[15] H. Zhang, Z. Ji, T. Xia, H. Meng, C. Low-Kam, R. Liu, S. Pokhrel, S. Lin, X. Wang, Y.-P. Liao, M. Wang, L. Li, R. Rallo, R. Damoiseaux, D. Telesca, L. Mädler, Y. Cohen, J. I. Zink, A. E. Nel, *ACS Nano* **2012**, *6*, 4349.

[16] C. Argyo, V. Weiss, C. Bräuchle, A. Bein Thomas E., *Chemistry of Materials* **2014**, *26*, 435.

[17] Y.-S. Lin, K. R. Hurley, C. L. Haynes, *The Journal of Physical Chemistry Letters* **2012**, 364.

[18] F. Tang, L. Li, D. Chen, *Adv. Mater.* **2012**, *24*, 1504.

[19] R. Narayan, U. Nayak, A. Raichur, S. Garg, *Pharmaceutics* **2018**, *10*, 118.

[20] Y. Chen, H. Chen, J. Shi, *Adv. Mater.* **2013**, *25*, 3144.

[21] Y. Zhao, B. G. Trewyn, I. I. Slowing, V. S.-Y. Lin, *J. Am. Chem. Soc.* **2009**, *131*, 8398.

[22] H.-J. Kim, H. Matsuda, H. Zhou, I. Honma, *Adv. Mater.* **2006**, *18*, 3083.

[23] C. Murugan, K. Rayappan, R. Thangam, R. Bhanumathi, K. Shanthi, R. Vivek, R. Thirumurugan, A. Bhattacharyya, S. Sivasubramanian, P. Gunasekaran, S. Kannan, *Sci Rep* **2016**, *6*, 34053.

[24] Q. Fu, D. Hargrove, X. Lu, *Nanomedicine: Nanotechnology, Biology and Medicine* **2016**, *12*, 1951.

[25] M. Ganesh, U. Ubaidulla, P. Hemalatha, M. M. Peng, H. T. Jang, *AAPS PharmSciTech* **2015**, *16*, 944.

[26] K. Möller, K. Müller, H. Engelke, C. Bräuchle, E. Wagner, T. Bein, *Nanoscale* **2016**, *8*, 4007.

[27] C. Tao, Y. Zhu, Y. Xu, M. Zhu, H. Morita, N. Hanagata, *Dalton Trans.* **2014**, *43*, 5142.

[28] G. V. Deodhar, M. L. Adams, B. G. Trewyn, *Biotechnol. J.* **2017**, *12*, 1600408.

[29] **N.d.**

[30] D. Bobo, K. J. Robinson, J. Islam, K. J. Thurecht, S. R. Corrie, *Pharmaceutical Research* **2016**, *33*, 2373.

[31] E. Phillips, O. Penate-Medina, P. B. Zanzonico, R. D. Carvajal, P. Mohan, Y. Ye, J. Humm, M. Gonen, H. Kalaigian, H. Schoder, H. W. Strauss, S. M. Larson, U. Wiesner, M. S. Bradbury, *Science Translational Medicine* **2014**, *6*, 260ra149.

[32] H. Yamada, C. Urata, Y. Aoyama, S. Osada, Y. Yamauchi, K. Kuroda, *Chemistry of Materials* **2012**, *24*, 1462.

[33] G. Chen, Z. Teng, X. Su, Y. Liu, G. Lu, *j biomed nanotechnol* **2015**, *11*, 722.

[34] L. Li, T. Liu, C. Fu, L. Tan, X. Meng, H. Liu, *Nanomedicine: Nanotechnology, Biology and Medicine* **2015**, *11*, 1915.

[35] M. Manzano, V. Aina, C. O. Areán, F. Balas, V. Cauda, M. Colilla, M. R. Delgado, M. Vallet-Regí, *Chemical Engineering Journal* **2008**, *137*, 30.

[36] V. Cauda, C. Argyo, T. Bein, *J. Mater. Chem.* **2010**, *20*, 8693.

[37] V. Cauda, A. Schlossbauer, T. Bein, *Microporous and Mesoporous Materials* **2010**, *132*, 60.

[38] Y.-S. Lin, N. Abadeer, K. R. Hurley, C. L. Haynes, *J. Am. Chem. Soc.* **2011**, *133*, 20444.

[39] S. P. Hadipour Moghaddam, R. Mohammadpour, H. Ghandehari, *Journal of Controlled Release* **2019**, *311–312*, 1.

[40] M. Vallet-Regí, F. Balas, D. Arcos, *Angew. Chem. Int. Ed.* **2007**, *46*, 7548.

[41] J. G. Croissant, Y. Fatieiev, N. M. Khashab, *Advanced Materials* **2017**, *29*, 1604634.

[42] T. Fontecave, C. Sanchez, T. Azaïs, C. Boissière, *Chemistry of Materials* **2012**, *24*, 4326.

[43] R. Mortera, S. Fiorilli, E. Garrone, E. Verné, B. Onida, *Chemical Engineering Journal* **2010**, *156*, 184.

[44] P. M. Dove, N. Han, A. F. Wallace, J. J. De Yoreo, *Proceedings of the National Academy of Sciences* **2008**, *105*, 9903.

[45] Q. He, J. Shi, M. Zhu, Y. Chen, F. Chen, *Microporous and Mesoporous Materials* **2010**, *131*, 314.

[46] E. Bindini, Z. Chehadi, M. Faustini, P.-A. Albouy, D. Grosso, A. Cattoni, C. Chanéac, O. Azzaroni, C. Sanchez, C. Boissière, *ACS Appl. Mater. Interfaces* **2020**, acsami.9b19956.

[47] R. O. Fournier, J. J. Rowe, *American Mineralogist* **1977**, *62*, 1052.

[48] G. B. Alexander, W. M. Heston, R. K. Iler, *The Journal of Physical Chemistry* **1954**, *58*, 453.

[49] S.-A. Yang, S. Choi, S. M. Jeon, J. Yu, *Scientific Reports* **2018**, *8*, 185.

[50] K. Braun, A. Pochert, M. Beck, R. Fiedler, J. Gruber, M. Lindén, *Journal of Sol-Gel Science and Technology* **2016**, *79*, 319.

[51] Y.-S. Lin, N. Abadeer, C. L. Haynes, *Chem. Commun.* **2011**, *47*, 532.

[52] S. Goel, F. Chen, S. Luan, H. F. Valdovinos, S. Shi, S. A. Graves, F. Ai, T. E. Barnhart, C. P. Theuer, W. Cai, *Adv. Sci.* **2016**, *3*, 1600122.

[53] J. D. Bass, D. Grosso, C. Boissiere, E. Belamie, T. Coradin, C. Sanchez, *Chemistry of Materials* **2007**, *19*, 4349.

[54] T. Asefa, Z. Tao, *Chem. Res. Toxicol.* **2012**, *25*, 2265.

[55] J. M. Rosenholm, V. Mamaeva, C. Sahlgren, M. Lindén, *Nanomedicine* **2012**, *7*, 111.

[56] P. Dogra, N. L. Adolphi, Z. Wang, Y.-S. Lin, K. S. Butler, P. N. Durfee, J. G. Croissant, A. Noureddine, E. N. Coker, E. L. Bearer, V. Cristini, C. J. Brinker, *Nat Commun* **2018**, *9*, 4551.

[57] F. Garbassi, L. Balducci, R. Ungarelli, *Journal of Non-Crystalline Solids* **1998**, *223*, 190.

[58] J. M. Kim, S. M. Chang, S. Kim, K.-S. Kim, J. Kim, W.-S. Kim, *Ceramics International* **2009**, *35*, 1243.

[59] F. Chen, S. Goel, H. F. Valdovinos, H. Luo, R. Hernandez, T. E. Barnhart, W. Cai, *ACS Nano* **2015**, *9*, 7950.

[60] F. Chen, K. Ma, L. Zhang, B. Madajewski, P. Zanzonico, S. Sequeira, M. Gonen, U. Wiesner, M. S. Bradbury, *Chem. Mater.* **2017**, *29*, 8269.

[61] T. M. Shaffer, M. A. Wall, S. Harmsen, V. A. Longo, C. M. Drain, M. F. Kircher, J. Grimm, *Nano Lett.* **2015**, *15*, 864.

[62] Q. He, Z. Zhang, F. Gao, Y. Li, J. Shi, *Small* **2011**, *7*, 271.

[63] D. S. Abou, T. Ku, P. M. Smith-Jones, *Nuclear Medicine and Biology* **2011**, *38*, 675.

[64] J. Lu, M. Liong, Z. Li, J. I. Zink, F. Tamanoi, *Small* **2010**, *6*, 1794.

[65] C.-H. Lee, S.-H. Cheng, Y.-J. Wang, Y.-C. Chen, N.-T. Chen, J. Souris, C.-T. Chen, C.-Y. Mou, C.-S. Yang, L.-W. Lo, *Adv. Funct. Mater.* **2009**, *19*, 215.

[66] J. S. Souris, C.-H. Lee, S.-H. Cheng, C.-T. Chen, C.-S. Yang, J. A. Ho, C.-Y. Mou, L.-W. Lo, *Biomaterials* **2010**, *31*, 5564.

[67] H. Meng, M. Xue, T. Xia, Z. Ji, D. Y. Tarn, J. I. Zink, A. E. Nel, *ACS Nano* **2011**, *5*, 4131.

Table of contents

The degradation kinetics and pathway of mesoporous silica nanoparticles (MSNs) are investigated *in vivo*, by tracking a radioactive label located either in the core or in the shell of PEGylated core-shell nanoparticles (NPs). The core-labeled NPs signal the location of the particles while the shell-labelled particles track the silica degradation products. A fast, hour-scale degradation kinetics is observed.

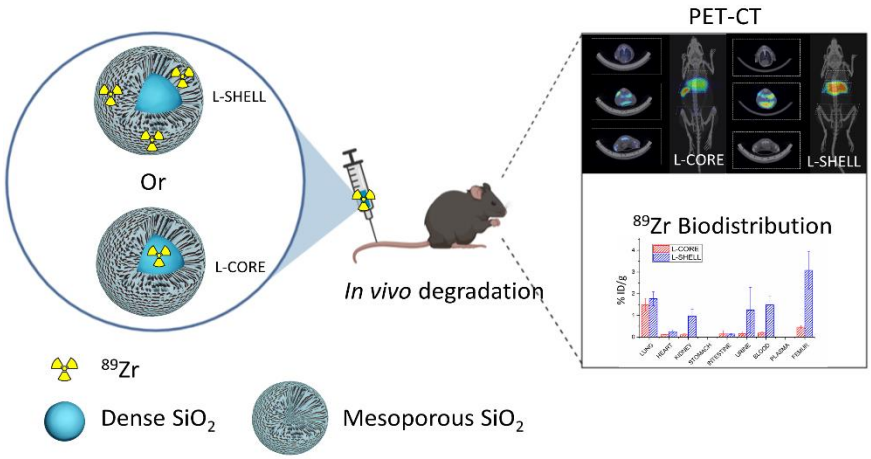

Figure 5: TOC

((Supporting Information can be included here using this template))

Supporting Information

Title ((no stars))

*Author(s), and Corresponding Author(s)** ((write out full first and last names))

((Please insert your Supporting Information text/figures here. Please note: Supporting Display items, should be referred to as Figure S1, Equation S2, etc., in the main text…)